Estimation of Blood Flow Velocity in the Heart of Fish Larvae Using Autocorrelation of Echocardiographic Signals

Sergey A. Titov* **and Lidia A. Zykova**
Federal State Budgetary Institution of Science "Scientific and Technological Centre of Unique Instrumentation" of the Russian Academy of Science, 15 Butlerova str., Moscow 117342, Russian Federation
*e-mail: sergetitov@mail.ru

Abstract. The paper is devoted to the estimation of blood flow velocity in the heart of a fish larva using a high-frequency ultrasonic scanner with a highly focused single-element ultrasonic transducer. The two-dimensional echocardiographic signal, recorded at a given probe position as a function of the delay of the reflected wave and time, is a superposition of randomly distributed responses reflected from moving blood cells. It is shown that a single value of flow velocity can be estimated by calculating the autocorrelation function of the echocardiographic signal, cropped by a two-dimensional data window. Moreover, for this purpose it is sufficient to calculate only the phase of the autocorrelation function at two adjacent points shifted by sampling intervals. The developed processing algorithm was verified using echocardiographic data measured on sturgeon larva aged 3 days after hatching. An ultrasonic transducer with a central frequency of 75 MHz, a bandwidth of 65%, and an angular aperture of 40° was used in the experiment. The velocity calculated in the ventricle area during one cardiac period varied in the range of ±10 mm/s depending on the contraction phase.

Keywords: ultrasonic focused transducer; sturgeon larva; M-scan; Doppler frequency shift; *in vivo* measurement.

Paper #9258 received 14 Mar 2025; revised manuscript received 22 Apr 2025; accepted for publication 29 Apr 2025; published online 27 Jun 2025. doi: 10.18287/JBPE25.11.020308.

1 Introduction

Echocardiography, which provides valuable information about the functioning of the cardiovascular system of living organisms, is widely used for clinical and research purposes [1]. In echocardiography, the spatio-temporal distribution of blood flow can be estimated by sending and receiving ultrasound waves [2, 3]. In modern medical scanners, the Doppler frequency shift of waves reflected by moving blood cells is used to determine the projection of the velocity vector onto the axis of the ultrasonic transducer [4, 5]. Some modern techniques make it possible to determine the velocity vector [6–8]. They are based on the rapid acquisition of two-dimensional scans and tracking the movement of blood cells in the longitudinal and transverse directions. The implementation of these techniques is impossible without the use of multi-element ultrasonic phased arrays. Since the heart of humans and other large living organisms is located deep in the body, the frequency range usually does not exceed 10 MHz, the angular aperture of the probing ultrasonic beam is narrow, and the spatial resolution is in a millimeter range. Higher resolution has been achieved in ultrasound examination of the heart of small animals such as mice and chickens [9–12]. Recently, high frequency echocardiography has been successfully applied in a wide range of works devoted to adult Zebrafish [13–15]. At the same time, it was shown that sonography of Zebrafish model at the embryonic and larval stages of development can be considered very promising for cardiological research [16–17]. Since the size of the fish heart at early stages of development is in the range of 200–300 μm [18], high frequency single element focused transducers were used in these works to ensure sufficient resolution. Due to short ultrasonic pulses with a central frequency in the range of 50–100 MHz and a wide angular aperture of the focused beam, the transverse and longitudinal resolution of the device was about 20 μm. This value is compatible with the typical size of the blood cells (7 μm) which give a strong stochastic reflected signal. Their velocity usually

does not exceed 10 mm/s, and the Doppler frequency shift in this case is too small for direct measurement in the spectral domain. The generation of echocardiographic signals from the Zebrafish larvae has been partly discussed in our previous work [19].

Typically echocardiographic signals are recorded in the M-scan format $s(t, T)$ [2, 3], where the "fast" time-of-flight t is associated with the propagation of the ultrasonic waves and the "slow" observation time T is associated with to the motion of the cardiac tissue. To determine the flow velocity, it is sufficient to measure the delays of ultrasonic echoes reflected from moving blood cells and, knowing the speed of sound in the liquid, calculate their displacement over a certain time interval T [2]. The delay can be obtained by isolating the pronounced echoes from others and using, for instance, the zero-crossing method. This approach is quite straightforward, but very often it is not possible to find a wavelet suitable for the analysis in the area of interest, especially using a fully automated software procedure.

A more advanced method of flow velocity estimation is based on the correlation approach. The relative delay of successive responses can be determined from the time shift of the peak of the one-dimensional cross-correlation function between one-dimensional or two-dimensional windowed data sets [2, 3]. This method has been successfully applied to study blood flow in fish larval hearts [16, 20], however a more reliable result could potentially be achieved using a two-dimensional autocorrelation approach [21].

It is shown that the velocity can be estimated from the phase of the two-dimensional autocorrelation function in the vicinity of its central lobe. This method is based on the assumptions that the velocity of moving cells does not change along the axis of the ultrasound beam and that its angular aperture is narrow. The efficacy of the two-dimensional autocorrelation technique was confirmed in a study of adult Zebrafish with a heart size of 1–2 mm [22]. Since moderate frequencies and angular apertures were used in this work, the assumptions made in developing the signal model should be considered acceptable. For small organism, highly focused high-frequency ultrasonic transducers are used, and the blood velocity varies with defocus distance, therefore the autocorrelation approach needs to be verified. In this paper, we present an autocorrelation method developed to estimate the blood flow velocity in the heart of fish at the larval stage of development.

2 Experiment

A high-frequency ultrasonic scanner was used to study the fish larval hearts *in vivo* (Fig. 1(a)). The device was equipped with a single element focused ultrasonic transducer with a central frequency of 75 MHz and a bandwidth of 65%. The angular aperture of the transducer was 40°, which provided a lateral resolution of approximately 20 μm. The transducer was excited by short (5 ns) electrical pulses and the signals reflected by the object were converted into digital form after filtration and amplification and stored in the computer. The position of the transducer relative to the object under study was controlled by a precise 3-axis mechanical scanner. To detect the temporal behavior of the heart at each transducer position (x, y), M-scans $s(t, T)$ were recorded for several seconds. The sampling periods of the digitized M-scans for the variables t and T were $\delta t = 2$ ns and $\delta T = 0.2$ ms, respectively. A more detailed description of the ultrasonic scanner can be found elsewhere [23].

In the experiment, sturgeon larva aged 3 days after hatching (Fig. 1(b)) was placed in an immersion cell filled with water. To immobilize the animal, a solution tricaine methane sulfonate (MS-222) at a concentration of 0.168 mg/L was used for anesthesia. The sagittal plane of the larva was oriented perpendicular to the z- axis of the transducer.

An example of M-scan $s(t, T)$ taken at point O of the heart (Fig. 1(b)) is shown in Fig. 2(a) as a grayscale image. The data are presented for one period of heart rhythm $T_0 = 0.454$ s. Several echo signals can be recognized in the images, the delays of which change with time T. The echoes M_1, M_2 are generated by the layered tissue of the myocardium, they show the upper and low walls of the heart chamber, respectively.

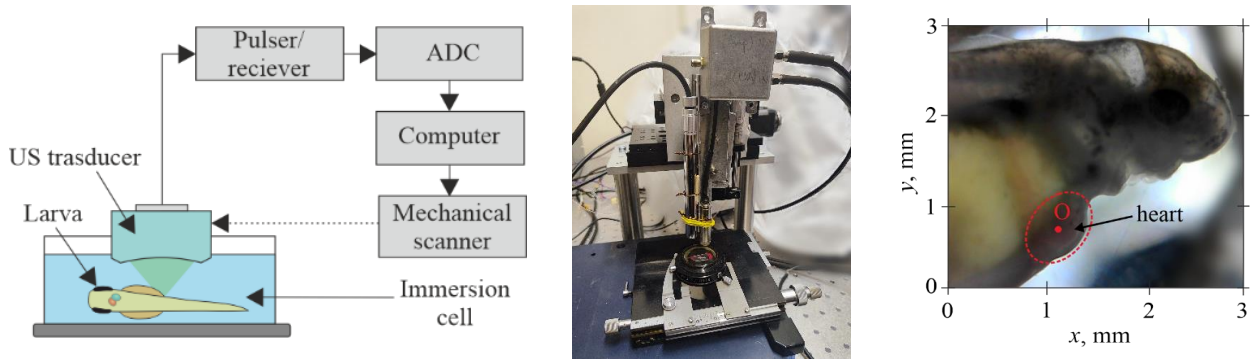

(a) (b) (c)

Fig. 1 (a) Scheme and (b) appearance of the experimental setup, (c) optical image of the heart area of the sturgeon larva.

The positions of these echoes change with time T in accordance with the heart contraction. Numerous noise-like B echoes result from scattering of the ultrasound probe wave by moving blood cells. Fig. 2(b) shows an enlarged fragment of this response, indicated in Fig. 2(a) by the yellow rectangle. The local slope of the wavelets B is proportional to the flow velocity V [2]. Indeed, during a time interval ΔT, blood cells, moving in the vertical direction and acquiring a delay Δt, travel a distance of $\Delta z = 0.5C{\cdot}\Delta t$, where $C \approx 1500$ m/s is the sound velocity in the tissue. Therefore, the velocity V can be estimated using a simple equation:

$$V = C\Delta t\left(2\Delta T\right)^{-1}. \qquad (1)$$

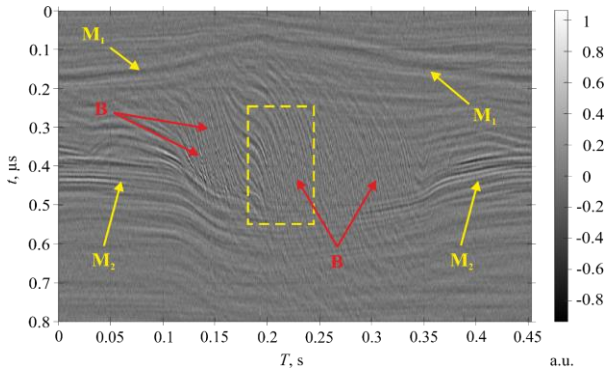

(a)

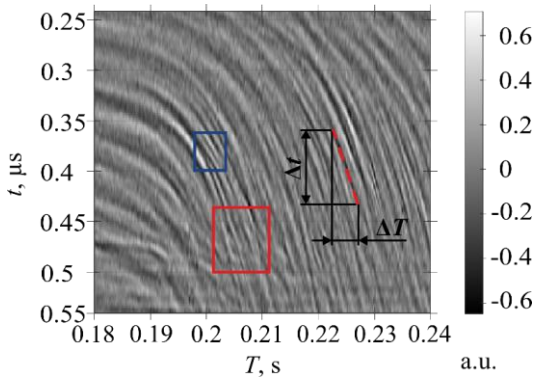

(b)

Fig. 2 (a) M-scan $s(t, T)$ recorded at the ventricle of the sturgeon larva. (b) Enlarged fragment of the scan marked in the (a) image with a yellow rectangle. B, M_1, M_2 are echo signals generated by blood cells, the upper and low walls of the heart chamber, respectively; Δt is the delay acquired by blood cells when moving along the red dotted line during the time interval ΔT.

The size of the blood components, mainly red blood cells, is about 5−10 μm, therefore there are approximately 10 reflectors in the resolution volume. The interference of the echoes from these randomly distributed cells forms a stochastic response B. Since the orientation and position of the reflectors change over time, the coherence duration is limited. Therefore, it is often impossible to find a wavelet that maintains integrity over the interval ΔT and to reliably estimate the delay Δt. A more robust estimate of the flow velocity can be obtained using a two-dimensional autocorrelation approach.

3 Theoretical Model of the Signal

To find the responses from the blood flow received by the ultrasonic transducer, the following assumptions can be accepted. The blood elements can be considered as point reflectors; their number is large within the focal volume. In the two-dimensional autocorrelation approach proposed in Ref. [21], it was assumed that the ultrasonic beam is wide, without a clear focal zone; and the spatial distribution of the velocity is axially symmetric and does not change along the axis. In the case of the tightly focused beam (Fig. 3), the signal $h\left(t,\bar{r},z\right)$ received from the reflector depends on time t and position $\left(\bar{r},z\right)$. The reflectors move at a velocity of $\overline{V_b} = \left(V,\overline{V}_r\right)$, where V and $\overline{V}_r$ are the vertical and radial components of the velocity vector. In a layer with a thickness of $2\Delta z$ and a center $z = z_a$, the velocity remains approximately constant during the observation time interval $|T| \le \Delta T$. Since the velocity of the blood cells is much less than the velocity of ultrasound waves in the tissue C, the response from the i-th moving particle can be written as follows:

$$s_i\left(t,T\right) = a_i h\left(t,\bar{r}_{0i} + \overline{V}_r T, z - z_{0i} - VT\right), \qquad (2)$$

where a_i is the reflection coefficient of the i-th particle, and $\left(\bar{r}_{0i}, z_{0i}\right)$ is its initial position at the moment T=0. The output signal is a sum of wavelets given in Eq. (2) whose response are in the time-of-flight interval $|t - t_a| \le \Delta t$, where $t_a = 2z_a C^{-1}$ and $\Delta t = 2\Delta z C^{-1}$.

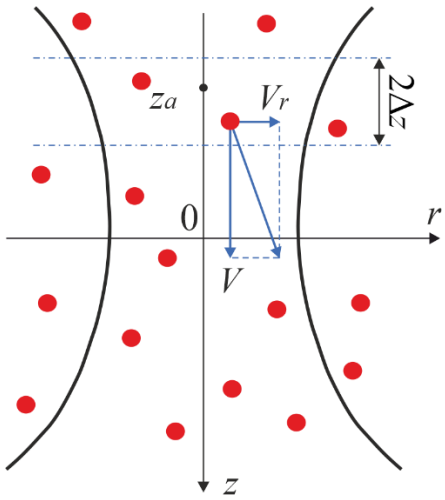

Fig. 3 The focal area of an ultrasonic beam containing an ensemble of moving particles. V and V_r are the vertical and radial components of the velocity; z_a and $2\Delta z$ are the position and the thicknes of the layer, respectively.

The wave fronts of the ultrasonic beam in the vicinity of the focus are approximately parallel to the focal plane [24], therefore motion of the particle along vertical axis z causes a delay of the reflected signal $2VTC^{-1}$. On the contrary, lateral motion does not change the signal delay, but it can change the amplitude of the signal. Since the delay is the same for all particles in the layer, the sum of their responses can be written as a two-dimensional convolution:

$$s_0(t,T)=\left[\sum_i a_i h_r\left(t,\bar{r}_{0i}+\bar{V}_r T, z-z_{0i}\right)\right]*\delta\left(t-\frac{2VT}{C}\right), \quad (3)$$

where $\delta()$ is the Dirac delta function. The function h_r shows the changes in the amplitude and delay of the temporal response $h(t)$ of the i-th reflector caused by its lateral displacement. The amplitude of the function h_r decreases smoothly as z_a deviates from the focal plane $z = 0$. The lateral displacement also causes amplitude variations determined by the profile of the ultrasonic beam. The duration of this response is limited by the travel time of the particle across the beam $\delta r/V_r$. Typically, the z-axis is oriented approximately along the blood flow so that $V_r << V$, and the particle remains inside the ultrasonic beam for the observation time interval ΔT. Summing the responses over the entire ensemble of the reflectors yields a stochastic function $g(t, T)$, and the output signal can be represented within the intervals Δt, ΔT as follows:

$$s(t,T)=\left[g(t,T)*\delta\left(t-\frac{2VT}{C}\right)\right]w_t(t)\,w_T(T), \quad (4)$$

where the window functions $w_T(T)$ and $w_t(t)$ cut out the data region intended for processing. In the observation intervals ΔT, Δt, the signal behavior is determined by the liner delay factor. This relationship given in Eq. (4) is equivalent to the signal model developed under other assumptions [18]. Using the methodology presented in this work, the following results can be obtained. The autocorrelation function $A(t, T)$ of a signal $s(t, T)$ can be found by taking the inverse Fourier transform of the signal power spectrum [25]:

$$A(t,T)=F^{-1}\left\{S(\omega,\Omega)S^*(\omega,\Omega)\right\}, \quad (5)$$

where the symbol * denotes the complex conjugation operation, and the frequencies ω, Ω are associated with the time variables t, T. The spectrum of the signal (Eq. 5) is equal to:

$$S(\omega,\Omega)=\left[G(\omega,\Omega)\cdot\delta\left(\Omega-\frac{2V}{C}\omega\right)\right]*W_\omega(\omega)*W_\Omega(\Omega), \quad (6)$$

where G, W_ω, W_Ω are spectra of g, w_t, w_T, respectively. In the case of infinite window functions w_t, w_T the convolution with W_ω, W_Ω in Eq. (6) can be omitted, and the spectrum $S(\omega, \Omega)$ is equal to 0 everywhere in the (ω, Ω) domain, except for the line $\Omega = 2VC^{-1}\omega$. Therefore, the variable Ω can be considered as the Doppler frequency shift obtained by the component of the probing wave with frequency ω due to reflection from the moving scatterer. The slope of this line depends on the velocity V, similarly the orientation of the components in the signal $s(t, T)$ and in its autocorrelation function $A(t, T)$ also depends on V. To estimate this slope, one can use the partial derivatives of the autocorrelation function with respect to the variables t and T.

In the case of infinite data windows, based on the definition of the Fourier integral and the properties of the delta function, the value of the derivative with respect to t of the autocorrelation function at the center (0, 0) is equal to:

$$r_t=\frac{\partial A(t,T)}{\partial t}_{t=0,T=0}= \\ =(2\pi)^{-2}\int_{-\infty}^{\infty}(-i\omega)\left|\left[G\left(\omega,\frac{2V}{c}\omega\right)\right]\right|^2 d\omega. \quad (7)$$

The partial derivative with respect to T can be obtained in a similar way:

$$r_T=\frac{\partial A(t,T)}{\partial T}_{t=0,T=0}=\frac{2V}{C}r_t. \quad (8)$$

Eq. (8) shows that the ratio of the coefficients r_T and r_t is proportional to the velocity V. In the case of finite data windows, the spectrum $S(\omega, \Omega)$ is smoothed due to the convolution given in Eq. (6), and Eq. (7) is invalid. However, it has been shown [21] that the coefficients r_T and r_t are the averaged values of the frequencies ω and Ω, respectively, and the relation given in Eq. (8) is applicable for estimating the velocity V.

It should be noted that digital calculation of derivatives of noisy experimental data may be unstable. However, since the amplitude and phase $\varphi(t, T)$ of the autocorrelation function are even and odd functions, respectively, the following approximation is valid:

$$\frac{\partial A(t,T)}{\partial t}_{t=0,T=0}=iA(0,0)\frac{\partial\varphi(t,T)}{\partial t}_{t=0,T=0}\approx \\ \approx iA(0,0)\frac{\varphi(\delta t,0)}{\delta t}, \quad (9)$$

where δt is the sampling period of the time-of-flight t. Using a similar relationship for the derivative with respect to the time T, Eq. (8) can be rewritten:

$$V=C\frac{\varphi(0,\delta T)\cdot\delta t}{2\varphi(\delta t,0)\cdot\delta T}, \quad (10)$$

where δT is the sampling period of the time T. Thus to estimate the velocity V at a specific point in the (t, T) domain it is sufficient to calculate the phase of the

autocorrelation function at two adjacent points shifted by intervals δt, δT.

4 Data Processing Algorithm

The experimental digital M-scan is a sampled version of the real valued signal presented as an n-by-m array $s_{nm} = s\left(n \cdot \delta t, m \cdot \delta T\right)$, where n and m are indexes related to the variables t and T, respectively. Before calculation of the autocorrelation function, the input data are converted to analytic signal $r_{nm} = s_{nm} + iH\left\{s_{nm}\right\}$, where i is the imaginary unit, and $H\{\}$ is the Hilbert transform with respect to n. To find the values of the autocorrelation function $A_{nm}^{(\delta t,0)}$ and $A_{nm}^{(0,\delta T)}$ at the lags (δt, 0) and (0, δT), respectively, first the element-wise products of the array r_{nm} and its shifted and complex conjugate copies are calculated:

$$\begin{aligned} D_{nm}^{(10)} &= r_{nm} \cdot r_{(n+1)m}^{*}, \\ D_{nm}^{(01)} &= r_{nm} \cdot r_{n(m+1)}^{*}. \end{aligned} \tag{11}$$

The signal power is calculated in a similar way:

$$D_{nm}^{(00)} = r_{nm} \cdot r_{nm}^{*}. \tag{12}$$

To find the values of the autocorrelation function, it is necessary to average the products given in Eq. (11) in sliding two-dimensional windows. This operation can be implemented using a low-pass two-dimensional finite impulse response filter w_{nm}:

$$\begin{aligned} A_{nm}^{(\delta t,0)} &= D_{nm}^{(10)} * w_{nm}, \\ A_{nm}^{(0,\delta T)} &= D_{nm}^{(01)} * w_{nm}, \\ A_{nm}^{(0,0)} &= D_{nm}^{(00)} * w_{nm}. \end{aligned} \tag{13}$$

The spatio-temporal distribution of the velocity V_{nm} can be obtained using the discrete version of Eq. (10):

$$V_{nm} = \frac{C\delta t \cdot \varphi\left(A_{nm}^{(0,\delta T)}\right)}{2\delta T \cdot \varphi\left(A_{nm}^{(\delta t,0)}\right)}. \tag{14}$$

The proposed algorithm is absolutely robust, since the output values V_{nm} can be calculated for all n and m for any input data s_{nm}. However, in many areas of the (n, m) domain there are no reflections from blood cells, and the signal-to-noise ratio is low. To exclude false results, the maximum value of the autocorrelation function $A_{nm}^{(0,0)}$ is compared with a certain threshold A_0. To mask these unreliable values the output is reset to 0: $V_{nm} = 0$, if $A_{nm}^{(0,0)} < A_0$.

It should be noted that the algorithm is computationally efficient. Indeed, it is sufficient to calculate only 3 values of the autocorrelation function given in Eq. (13) for each output value V_{nm}. In the case of a boxcar window w_{nm}, basically only $N_f \cdot M_f$ sum operations are required, where N_f, M_f are the window sizes. In contrast, in the one-dimensional cross-correlation algorithm, it is necessary to calculate the correlation function and find its peak for each point in the (t, T) domain.

The implementation of the two-dimensional autocorrelation approach presented in the works [21, 22] is based on demodulation of received signals and digital processing of quadrature components. In the present work, the bandwidth of the signal is wide, so the analog demodulation is ineffective. The velocity estimation accuracy is expected to remain the same since both algorithms are mathematically equivalent. However, additional threshold processing provides greater stability of results for small larval hearts, where it is difficult to locate cardiac chamber boundaries and exclude areas with low signal-to-noise ratio.

5 Results and Discussion

The estimated spatio-temporal distribution of blood flow velocity V is shown in Fig. 4. The calculation was performed using the input M-scan data shown in Fig. 2. The velocity value is color-coded according to the color scale shown on the right side of the picture. The threshold was equal to $A_0 = 0.36 \cdot A_{max}$, where A_{max} is the global maximum of the autocorrelation function $A_{nm}^{(0,0)}$. The window sizes were set equal to $N_f = 16$ and $M_f = 20$. These numbers correspond to the window (32 ns) by (4 ms) indicated in the (t, T) domain by a blue rectangular (Fig. 2(b)). This window is small enough compared to the time range t (≈600 ns) and the heart rhythm period $T_0 = 0.454$ s to correctly show the change in velocity V depending on the vertical position and the phase of the heart contraction.

At two intervals of the time T = (0.12−0.15) s and T = (0.2−0.24) s (Fig. 4) the blood flow is directed downwards, where the velocity reaches a peak value of V ≈ –15 mm/s. At the intervals T = (0−0.12) s, (0.15−0.2) s and (0.41-0.45) s, the movement of blood cells is slowed down. During a short time interval T = (0.35−0.37) s and in the time-of-flight interval t = (0.38−0.41) μs, a strong upward flow is observed with a peak velocity of +15 mm/s. Outside the cardiac chamber, where the time-of-flight t < 0.15 μs or t > 0.55 μs, the signal is weak, the autocorrelation function is less than the threshold A_0, and the output was set to 0. Overall, the behavior of the calculated blood flow velocity is in good agreement with the original M-scan (Fig. 2).

The blue graph in Fig. 5 shows the calculated velocity $V(T)$ taken at time t = 0.385 μs along the red dashed line (Fig. 4). The calculation was repeated using the 2D window sizes increased from $N_f \cdot M_f$=16·20 to $N_f \cdot M_f$=32·40 gives (red graph). These windows, superimposed on the measured data $s(t, T)$ are presented in Fig. 2(b) as blue and red rectangles, respectively, to illustrate their relative sizes. It can be concluded that a

larger window decreases the level of fluctuations, but also reduces the resolution due to data smoothing.

The velocity $V(T)$ was also estimated by directly applying Eq. (1) to the raw data $s(t, T)$. Measurement of Δt and ΔT was not possible in all points in the (t, T) domain due to the stochastic nature of the signal. Successfully obtained velocity estimates are presented in Fig. 5 as green crosses. There is good agreement between these values and the results of the autocorrelation approach which confirms correctness of the proposed algorithm.

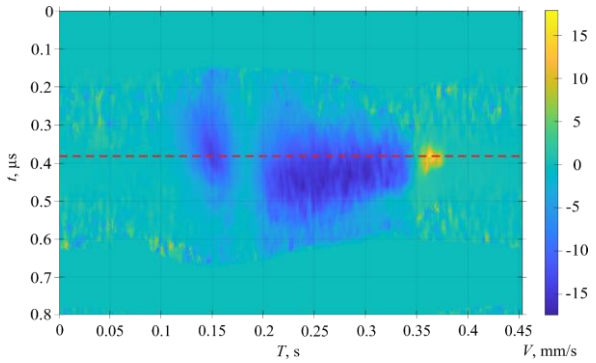

Fig. 4 The velocity $V(t, T)$ calculated using M-scan shown in Fig. 2.

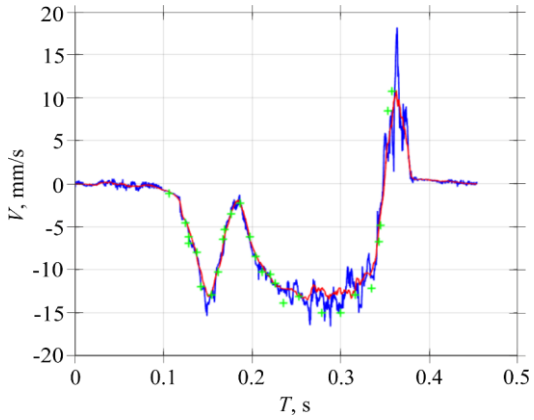

Fig. 5 Velocity $V(t_0, T)$, $t_0 = 0.385$ μs. The window sizes are 32 ns × 4 ms and 64 ns × 8 ms (blue and red graphs, respectively). Velocity V estimated using Eq. (1) (green crosses).

6 Conclusion

In this work, an algorithm for processing high-frequency echocardiographic signals recorded using a focused single-element ultrasonic transducer is developed. The algorithm can be used to estimate the spatiotemporal distribution of blood flow velocity in the hearts of small animals, such as fish larvae. To obtain sufficient robustness of the estimation, it is based on two-dimensional autocorrelation analysis of stochastic echocardiographic signals. It is shown that to obtain the value of velocity at a specific point of the heart and for a specific moment of the cardiac period, it is sufficient to calculate only two values of the autocorrelation function. The data used for the calculation are cropped by a local two-dimensional window. The window size is a trade-off between resolution and estimation accuracy. The algorithm is absolutely robust, but it is possible to obtain incorrect values outside the cardiac chambers where the signal to-noise ratio is low. To avoid this, the output value is excluded if the maximum of the autocorrelation function is less than a certain threshold. The developed technique is verified using echocardiographic signals measured *in vivo* in sturgeon larvae. However, it can also be applied to other species with small cardiovascular systems that require the use of a single element focused transducer to obtain high spatial resolution.

All procedures were approved by the Bioethics Committee of the Scientific and Technological Centre of Unique Instrumentation of the Russian Academy of Sciences (STC UI RAS), protocol #1/25, dated 24 February 2025.

Acknowledgment

This study was supported by Federal State Task Program of STC UI RAS (FFNS-2025-0008).

Disclosures

All authors declare that there is no conflict of interest in this paper.

References

1. P. Nihoyannopoulos, J. Kisslo (Eds.), Echocardiography, 2nd Ed., Springer Cham, Switzerland (2018). e-Book ISBN: 9783319716176.
2. T. L. Szabo, Diagnostic ultrasonic imaging inside out, 2nd Edition, Academic Press, Oxford, UK (2014). ISBN: 9780123964878.
3. K. K. Shung, Diagnostic ultrasound: imaging and blood flow measurements, 1st Ed., CRC Press, Boca Raton, FL, USA (2006). eBook ISBN: 9780429147449.
4. I. A. Hein, W. D. O'Brien, "Current time-domain methods for assessing tissue motion by analysis from reflected ultrasound echoes-a review," IEEE Transactions on Ultrasonics, Ferroelectrics, and Frequency Control 40(2), 84–102 (1993).
5. G. Guidi, C. Licciardello, and S. Falteri, "Intrinsic spectral broadening (ISB) in ultrasound Doppler as a combination of transit time and local geometrical broadening," Ultrasound in Medicine & Biology 26(5), 853–862 (2000).

6. J. Baun, "Emerging technology: Ultrasound vector flow imaging—a novel approach to arterial hemodynamic quantification," Journal of Diagnostic Medical Sonography 37(6), 599–606 (2021).
7. J.A. Jensen, S.I. Nikolov, A.C. Yu, and D. Garcia, "Ultrasound vector flow imaging-part I: sequential systems," IEEE Transactions on Ultrasonics, Ferroelectrics, and Frequency Control 63(11), 1704–1721 (2016).
8. A. Goddi, M. Fanizza, C. Bortolotto, M. V. Raciti, I. Fiorina, X. He, Y. Du, and F. Calliada, "Vector flow imaging techniques: An innovative ultrasonographic technique for the study of blood flow," Journal of Clinical Ultrasound 45(9), 582–588 (2017).
9. L. Sun, W. D. Richard, J. M. Cannata, C. C. Feng, J. A. Johnson, J. T. Yen, and K. K. Shung, "A high-frame rate high-frequency ultrasonic system for cardiac imaging in mice," IEEE Transactions on Ultrasonics, Ferroelectrics, and Frequency Control 54(8), 1648–1655 (2007).
10. J. G. Vilches-Moure, "Embryonic chicken (Gallus gallus domesticus) as a model of cardiac biology and development," Comparative Medicine 69(3), 184–203 (2019).
11. F. M. Benslimane, M. Alser, Z. Z. Zakaria, A. Sharma, H. A. Abdelrahman, and H. C. Yalcin, "Adaptation of a mice doppler echocardiography platform to measure cardiac flow velocities for embryonic chicken and adult zebrafish," Frontiers in Bioengineering and Biotechnology 7, 96 (2019).
12. S. Ho, G. X. Y. Tan, T. J. Foo, N. Phan-Thien, and C. H. Yap, "Organ dynamics and fluid dynamics of the HH25 chick embryonic cardiac ventricle as revealed by a novel 4D high-frequency ultrasound imaging technique and computational flow simulations," Annals of Biomedical Engineering 45(10), 2309–2323 (2017).
13. L. Lee, C. E. Genge, M. Cua, X. Sheng, K. Rayani, M. F. Beg, M. V. Sarunic, and G. F. Tibbits, "Functional assessment of cardiac responses of adult zebrafish (danio rerio) to acute and chronic temperature change using high-resolution echocardiography," PLoS ONE 11(1), e0145163 (2016).
14. A. Evangelisti, K. Schimmel, S. Joshi, K. Shah, S. Fisch, K. M. Alexander, R. Liao, and I. Morgado, "High-frequency ultrasound echocardiography to assess Zebrafish cardiac function," JoVE: Journal of Visualized Experiments 157, 60976 (2020).
15. C.-C. Chang, P.-Y. Chen, H. Huang, and C.-C. Huang, "In vivo visualization of vasculature in adult zebrafish by using high-frequency ultrafast ultrasound imaging," IEEE Transactions on Biomedical Engineering 66(6), 1742–1751 (2019).
16. S. A. Titov, A. B. Burlakov, A. N. Bogachenkov, "Sonography of the heart of weatherfish misgurnus fossilis at the prelarval stage of development," Acoustical Physics 67(5), 562–570 (2021).
17. A. S. Machikhin, S. A. Titov, C.-C. Huang, A. V. Guryleva, A. B. Burlakov, L. A. Zykova, and V. I. Bukova, "Combined optical and acoustic microscopy for noninvasive cardiovascular studies using zebrafish model," IEEE Transactions on Instrumentation and Measurement 74, 1–13 (2025).
18. S. F. Gilbert, M. J. F. Barresi, Developmental Biology, 11th Ed., Sinauer Associates, Sunderland, MA (2016).
19. S. A. Titov, L. A. Zykova, "Estimation of particle flow velocity in a liquid from pulse echo signals of an ultrasonic focusing transducer," IEEE Xplore: 2024 Wave Electronics and its Application in Information and Telecommunication Systems (WECONF), 1–4 (2024).
20. S. A. Titov, L. A. Zykova, A. B. Burlakov, and C. C. Huang, "Estimation of blood flow velocity in the heart of the danio rerio embryo using correlation of ultrasonic signals," in 2022 International Conference on Information, Control, and Communication Technologies (ICCT), 1–4 (2022).
21. T. Loupas, R. W. Gill, and R. B. Peterson, "Experimental evaluation of velocity and power estimation for ultrasound blood flow imaging, by means of a two-dimensional autocorrelation approach," IEEE Transactions on Ultrasonics, Ferroelectrics, and Frequency Control 689–699 (1995).
22. C.-C. Huang, T.-H. Su, and C.-C. Shih, "High-resolution tissue doppler imaging of the zebrafish heart during its regeneration," Zebrafish 12(1), 48–57 (2015).
23. A. B. Burlakov, S. A. Titov, and A. N. Bogachenkov, "Application of acoustic microscopy for visualization of structural displacement during the development of fish embryos," Journal of Communications Technology and Electronics 67(4), 456–462 (2022).
24. L. R. Gavrilov, High Intensity Focused Ultrasound in Medicine, Phasis, Moscow (2013). [in Russian]
25. A. Papoulis, Systems and Transforms with Applications in Optics, Krieger, Malabar, Florida, USA (1986). ISBN: 978-0898743586.